

# Simulating CRF with CNN for CNN

Lena Gorelick

Olga Veksler

May 7, 2019

## Abstract

Combining CNN with CRF for modeling dependencies between pixel labels is a popular research direction. This task is far from trivial, especially if end-to-end training is desired. In this paper, we propose a novel simple approach to CNN+CRF combination. In particular, we propose to simulate a CRF regularizer with a trainable module that has standard CNN architecture. We call this module a CRF Simulator. We can automatically generate an unlimited amount of ground truth for training such CRF Simulator without any user interaction, provided we have an efficient algorithm for optimization of the actual CRF regularizer. After our CRF Simulator is trained, it can be directly incorporated as part of any larger CNN architecture, enabling a seamless end-to-end training. In particular, the other modules can learn parameters that are more attuned to the performance of the CRF Simulator module. We demonstrate the effectiveness of our approach on the task of salient object segmentation regularized with the standard binary CRF energy. In contrast to previous work we do not need to develop and implement the complex mechanics of optimizing a specific CRF as part of CNN. In fact, our approach can be easily extended to other CRF energies, including multi-label. To the best of our knowledge we are the first to study the question of whether the output of CNNs can have regularization properties of CRFs.

## 1 Introduction

The advances in Convolutional Neural Networks (CNNs) [18, 28, 26, 31] lead to a tremendous success in computer vision recently. CNNs excel at learning reliable features for a multitude of vision problems. Originally designed for classification of an entire image, CNNs have been extended to tasks where each image pixel is

assigned a class label, such as semantic segmentation [12, 30], stereo correspondence [35, 11], optic flow [16], etc. While the labels produced by CNN at nearby pixels are correlated, due to the overlap of their receptive fields, such dependencies are not explicitly modeled. Therefore, to improve the precision of pixel labeling, CNNs are often combined with Conditional Random Fields (CRFs) [27, 25]. CRFs were designed for and excel at the task of modeling various pixel label dependencies. CRF models, however, are not easy to incorporate with CNNs. There are various prior approaches.

The simplest approach to combine CNN and CRF is to apply CRF as post processing [12, 9]. In these approaches, the probabilities for class labels learned by CNN are converted into the unary CRF terms. Then a CRF optimization algorithm, such as in [6, 25] is used to obtain the final labeling. While simple, this approach does not support end-to-end training. The unary terms learned by CNN may not be the best tailored to the separate CRF optimization step.

Another approach is to implement a CRF optimizer as part of the neural network. In [37], they show how to implement mean-field inference [24], a popular technique for optimizing full CRFs, as a Recurrent Neural Network (RNN). This approach supports end-to-end training, as CRF is integrated into the system architecture. The limitation is that the CRF is fixed to the Gaussian-edge CRF from [25], and the optimizer is fixed to the mean-field inference. If another CRF and/or optimizer is desired, the architecture has to be hand-designed from scratch, which is technically difficult.

Yet another approach is to use the structured prediction learning framework [10, 23]. Here the unary and/or pairwise potentials of a CRF are modeled with CNN-computed features. This approach supports end-to-end training. The difficulty here is optimization of the structured loss function. Computing the exact gradient of the loss is usually infeasible and has to be approximated. If CRF is restricted to be Gaussian, then inference is an easier task [7, 34, 8]. However, the class of Gaussian CRFs is rather limited.

We propose a simple approach for combining CNNs with CRFs in one end-to-end trainable system. Our main idea is a special *CRF Simulator* module. This module is built using standard CNN architecture and simulates the performance of a CRF regularizer. It is trained from data with ground truth obtained from an actual CRF optimizer. In particular, the input to CRF Simulator are the unary and pairwise terms of a CRF. The output is the simulation of a labeling that an actual CRF optimizer would produce.

Note that our CRF Simulator module is trained to produce a labeling similar to that of an actual CRF optimizer, as opposed to training that aims to produce a

low energy labeling. Thus at no point during training we compute an actual CRF energy. CRFs are used to produce a regularized labeling, for example a labeling with a short boundary, low boundary curvature, etc. We can train a CRF-simulator that learns to produce a regularized labeling without an explicit knowledge of the energy function, just from observing the regularization effect on the training samples.

While our approach requires labeled data, fortunately, a virtually unlimited amount of training data can be generated given an efficient actual CRF optimizer. Once trained, CRF Simulator is seamlessly incorporated as a part of any larger CNN architecture. Our approach enables end-to-end training, namely the parameters of the other modules are learned with consideration of the CRF Simulator module behavior.

Another advantage of our approach is the ease of incorporating novel/different CRF models. This is because our CRF Simulator is based on a standard CNN architecture. If we wish to implement a new CRF regularizer, all we need to do is generate a new training dataset and re-train the CRF Simulator. This is possible when there is an efficient optimizer available for the CRF of choice. Note that retraining a CRF simulator is significantly easier in practice, compared to prior work, where they have to develop a new technical approach for each new CRF model.

Regularizing and optimization [32, 21] is a large and well-established area of computer vision. Multiple regularizers and their properties were studied, as well as multiple optimization algorithms were developed over the past four decades. It is an interesting question to ask if regularization properties can be simulated by CNNs, without actually performing optimization. As far as we know, our work is the first one to look at this question.

We experimentally validate our proposed approach on the task of salient object segmentation. This is a particularly suitable case since it requires optimization of binary CRF energy. The ground truth data for training our CRF simulator is obtained efficiently and exactly by a graph cut algorithm [5]. Our approach can be easily extended to the multi-label case by applying multi-label optimization algorithms to generate the ground truth for our simulator. Fortunately, the area of efficient CRF optimization is vast and there are many options available, see [32, 21] for a review.

This paper is organized as follows. In Sec. 2, we review the related work. In Sec. 3, we describe our CRF Simulator design. In Sec. 5.2 we show how to use a CRF Simulator as a part of a complete CNN system. Experimental results are in Sec. 5 and the conclusions and future work are in Sec. 6.

## 2 Related Work

The work in [12] was among the first to use a CRF for post-processing of the results obtained with CNN. In particular, they use CNNs as a multi-scale feature extractor over superpixels. They form a superpixel-based CRF, and obtain the final segmentation using the expansion algorithm from [6]. The work in [9] uses the Fully Convolutional Networks (FCN) from [30] to learn the unary terms for a Gaussian edge full-CRF [25]. Then mean field annealing is used for CRF inference as a post-processing step. While simple, these approaches do not support end-to-end training. The CRF parameters are not learned from the training data together with CNN parameters.

Another interesting approach that also uses Gaussian-edge full CRFs from [25] is in [37]. They show how to implement mean-field inference [24], a popular technique for optimizing full CRFs, as a Recurrent Neural Network (RNN). This approach is capable of end-to-end training, as CRF is integrated into the architecture of the whole system. Later, they extended their approach to handle higher order CRF terms [2]. There are numerous other extensions to this RNN-CNN approach, such as bilateral neural network for high dimensional sparse data [20], more effective CRF optimization based on linear programming LP [1] or continuous relaxation [14]. Also see [3] for a recent overview of the approaches that follow this direction.

While powerful, the RNN-CNN approach requires hand-designing special architecture for each new CRF one wishes to model. This is a very difficult task, and thus far, other than CRF model with mean field optimization, there are few other examples. The only other example we are aware of is the work of [15], that describe how to implement a submodular CRF layer within a CNN architecture. Their approach is technically difficult and is limited to submodular functions.

In [10], they model MRF potentials as deep features using a structured learning framework. In this framework, computing exact gradient descent updates is computationally infeasible, and they resort to various approximations, such as using local belief functions instead of the true marginals. While theoretically interesting and amenable to end-to-end training, their approach relies on a number of approximations and is complex to implement.

In [23], they also proposed a method for CRF-CNN training based on structured learning. Like [10], the main difficulty of this approach is efficiently back-propagating through the CRF module. For each specific CRF model, a new approach has to be developed from scratch.

An alternative approach is to incorporate regularization directly into the loss

function. For example the approach in [33] incorporates normalized cut regularization into the loss function for the problem of weakly supervised learning. However, incorporating length regularization into loss during fully supervised learning surprisingly leads to inferior performance compared with unregularized loss function<sup>1</sup>, also confirmed by our experiments.

### 3 CRF Simulator

In this section we describe the design of our CRF Simulator. Even though we present the case of binary CRF energy for the task of salient object segmentation, our proposed approach is general and can be easily extended to other energies and applications. In Sec. 3.1 we describe the CRF energy function that we seek to simulate. In Sec. 3.2 we give details of the CNN architecture for our CRF Simulator. In Sec. 3.3 we explain how we automatically generate the training data.

#### 3.1 CRF Energy Function

The energy function in this section is the one proposed in [4] for segmenting an object from the background. Let  $\mathcal{P}$  be the set of image pixels, and  $x_p \in \{0, 1\}$  be the label assigned to pixel  $p$ . Here label 0 corresponds to the background, and 1 to the salient object. Let  $\mathbf{x} = (x_p \mid p \in \mathcal{P})$  be a vector storing labels for all pixels. The CRF energy that we wish to simulate is defined as

$$f(\mathbf{x}) = \sum_{p \in \mathcal{P}} f_p(x_p) + \sum_{p, q \in \mathcal{P}} w_{pq} \cdot [x_p \neq x_q], \quad (1)$$

The unary terms  $f_p(x_p)$  give the cost of assigning pixel  $p$  to label  $x_p$ . We model them as negative log probabilities for salient object and background. The pairwise terms  $w_{pq} \cdot [x_p \neq x_q]$  penalize label discontinuities between neighboring pixels. We set  $w_{pq}$  to be inversely proportional to the color difference of pixels  $p$  and  $q$

$$w_{pq} = \lambda \cdot \exp\left(-\frac{\|C_p - C_q\|^2}{2\sigma^2}\right). \quad (2)$$

This type of CRF energy function regularizes a labeling by encouraging a shorter boundary length. The larger is the  $\lambda$ , the stronger is the regularizer influence in comparison to the unary terms.

---

<sup>1</sup>Private communication with the authors

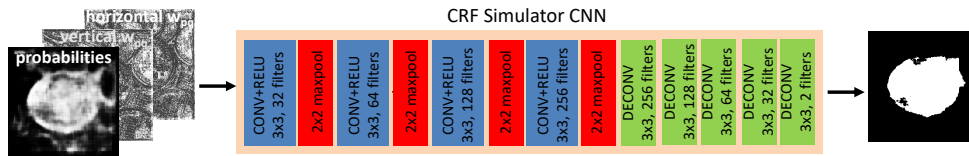


Figure 1: Architecture of CRF Simulator CNN.

The optimum labeling minimizing the energy in Eq. (1) can be found via the minimum cut algorithm [5]. Thus this energy function is particularly suitable for an initial evaluation of our approach since we can generate globally optimum labelings for our ground truth dataset.

### 3.2 CNN Architecture

To train our CRF Simulator, we use the network illustrated in Fig. 1. The input is 3-channel “image” where the first channel stores the unary terms of the energy function in Eq. (1) and the other two channels store horizontal and vertical pairwise terms respectively. The output is the regularized labeling. The architecture is a standard Encoder-Decoder one, with four convolutional and deconvolutional layers. This simple network achieves 90.44% F-measure on the test data. We also tried to get a better performance by using features from the VGG network [31] pretrained on ImageNet [13]. However, such network had a slightly inferior performance. The likely explanation is that VGG network is pretrained on real world images, whereas the input to CRF Simulator CNN is of different type.

### 3.3 Training Data

The input to our CRF Simulator is the unary and pairwise terms of the energy in Eq. (1). First we describe the input unary terms. For training our CRF-simulator, we wish to have a richer class of optimization problems than just those coming from saliency. Therefore we combine two data sets: the MSRA-B dataset [36] and PASCAL data set 2012 [17]. We divide MSRA-B data set into 2500 images for training, 500 for validation, and 2000 for testing. Similarly, we take the first 80% images from PASCAL database for training, the next 10% for validation and the last 10% for testing giving subsets of (13700, 1712, 1712) images respectively.

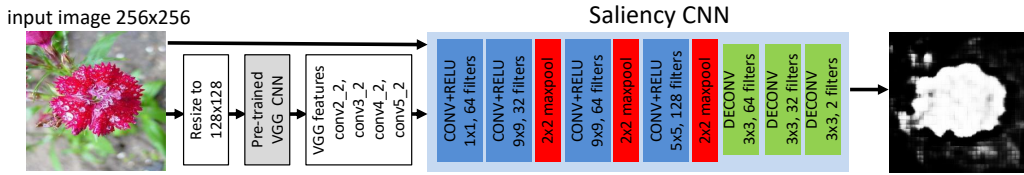


Figure 2: Architecture of Saliency CNN.

We then obtain input unary terms using two different procedures, one for images from MSRA-B data set, where the data terms are based on pixel saliency, and one for images from PASCAL data set, where the data terms are based on appearance.

In the first case we use the training subset of MSRA-B to train a separate Saliency-CNN component shown in Fig. 2. For each input image it outputs saliency probability map. This probability map is subsequently used as an input to the CRF Simulator. See Sec. 4.1 for detailed description of Saliency-CNN.

In the second case, for each PASCAL image we create multiple instances of input data-terms. For any image  $i$  that has an object segmentation map provided with the data set, we compute data-terms  $\mathbf{f}_i^k(\mathbf{x})$  separately for each object mask  $k$  as follows. First, we fit an appearance model for foreground and background of each mask  $k$  using discrete normalized color histograms with 16 bins per channel. We then normalize the resulting data terms to sum to one for each pixel. For images in PASCAL that do not have object segmentation masks we fit histograms to four random rectangular regions. This process results in several instances of data terms  $\mathbf{f}_i^k$  per image, yielding additional (50068, 6852, 6852) input images for training, validation and testing of our CRF Simulator respectively.

During training, we use a set of 30 different  $\lambda$  values, ranging from 0 to 400. These values are sampled more densely in the lower range, since lower values of  $\lambda$  lead to a better segmentation more frequently. When  $\lambda = 400$ , for all images in our dataset the CRF-optimizer produces an empty labeling. Thus  $\lambda = 400$  is a sufficiently large value to ensure CRF Simulator learns the extreme case when the object is completely smoothed out by the regularizer.

The training examples for our CRF Simulator are “images” with three channels. The first channel stores the unary terms as described above: either from Saliency CNN in Fig. 2 or from fitting appearance models to segmentation masks in the PASCAL dataset. The second and third channels are the horizontal and vertical terms  $w_{pq}$  respectively, vectorized as two images. energy in Eq. (1) com-

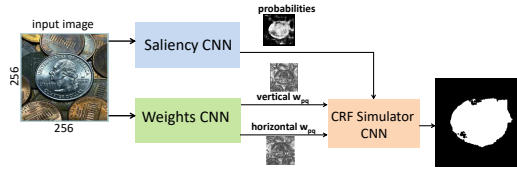


Figure 3: Complete system overview.

pletely. To generate the ground truth for each training example, we simply run the min-cut/max-flow algorithm of [5] producing the labeling of the lowest energy. We use training, validation and test subsets from MSRA-B dataset, and 30 different values of  $\lambda$  to generate 75,000 training, 15,000 validation and 60,000 test examples for our CRF Simulator. Similarly, for images from PASCAL dataset we run max-flow to produce labeling for 16 different values of  $\lambda$  and randomly choose five of them to generate additional 250340, 34260 and 34260 examples for training, validation and testing respectively.

## 4 Complete System

We now describe how we use our CRF Simulator in a complete system for segmenting salient objects, see Fig. 3. Our system has three main components: Saliency-CNN, Weights-CNN and CRF Simulator CNN. Components are illustrated in detail in Fig. 2, Fig. 4 and Fig. 1 respectively. The input image first goes through Saliency-CNN which outputs a single channel of saliency probability map. The original image is also used as input to the Weights-CNN component which outputs two channels of vertical and horizontal smoothness terms  $w_{pq}$ . Then, the saliency probabilities and the smoothness terms are concatenated and fed as input to the pre-trained CRF Simulator CNN which outputs regularized segment of the salient object.

Before training the complete system we initialize CRF Simulator module with the weights obtained during the separate training stage on the CRF Simulator dataset described in Sec. 3.3. Similarly, Saliency CNN weights are initialized with the weights obtained during separate training on the MSRA-B saliency dataset. The parameters of the Weights CNN module are initialized randomly. During training, we can choose to either keep the weights of CRF Simulator and Saliency CNN fixed, or allow them to be further tuned. We evaluate these options in Sec. 5.



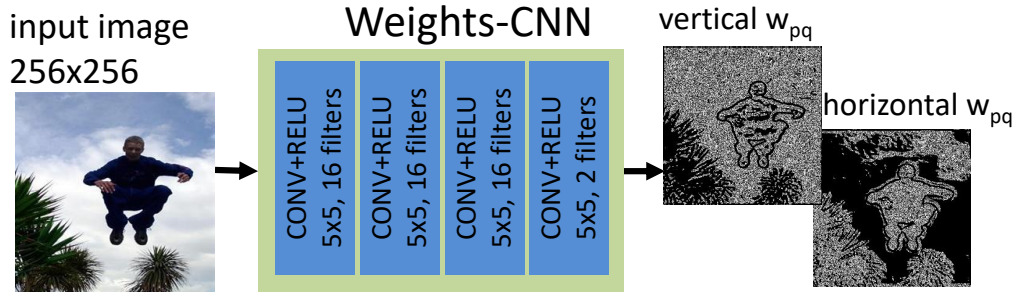


Figure 4: Module for obtaining  $w_{pq}$  for the complete system.

## 4.1 Saliency-CNN

Given an input image, the role of the Saliency-CNN is to output a salience map. Our architecture for this module is in Fig. 2. We make use of the VGG network [31] pre-trained on ImageNet [13]. The input image is resized to 128x128 and fed into VGG CNN. We then use VGG features in a manner similar to [29]. Namely, we extract conv2\_2, conv3\_2, conv4\_2 and conv5\_2, upscale them to the original size and concatenate to the original image. Similarly to [29] we reduce the dimensionality by performing one layer of 1x1 convolution which results in 64 features. We then use a standard Encoder-Decoder network, with four convolutional and deconvolutional layers as shown in Fig. 2. The output is a salience probability map. Our network achieves F-measure of 88.21% on the MSRA-B dataset. The state of the art performance is close to F-measure of 93% [19]. Our network is relatively close to the state of the art, and offers a good compromise in terms of its size.

## 4.2 Weights-CNN

The idea of Weights-CNN component is that the smoothness terms and the strength of regularization useful for CRF Simulator can be learned directly from the image. Our architecture for this component is in Fig. 4. It takes the input image and performs four sets of 5x5 convolutions. The last layer outputs two channels. The first one is taken to be the vertical  $w_{pq}$ , and the last channel the horizontal  $w_{pq}$ . Although there is no explicit  $\lambda$  parameter, the strength of regularization is implicitly learned through the relative magnitude of weights  $w_{pq}$ : the larger are  $w_{pq}$ , the more regularization CRF Simulator will produce.

## 5 Experimental Results

We used the MSRA-B saliency dataset from [36] to evaluate our complete system. We divided it randomly into 2500 images for training, 500 for validation, and 2000 for testing. We re-scaled all images to be of size 256 by 256.

We use the  $F$ -measure as the main criteria for performance evaluation, since this is the customary measure for salient object segmentation. Let  $P$  be the precision (i.e. the percentage of pixels that are correctly labeled as object out of all pixels labeled as object), and  $R$  the recall (i.e. the percentage of pixels that are correctly labeled as object out of all object pixels). Then  $F$ -measure is defined as

$$F_{\beta} = (1 + \beta^2) \frac{P \cdot R}{\beta^2 \cdot P + R}. \quad (3)$$

We set  $\beta^2 = 0.3$ .

The dataset for training CRF Simulator contains some cases where the ground truth has no object pixels. This happens when  $\lambda$  value is too high. In these cases, the  $F$ -measure is not well defined. To fix this problem, we reverse the meaning of object and background when computing the  $F$ -measure for such examples. Intuitively, this makes sense since for such examples, the most accurate answer is to label every single pixel as “background”.

All CNNs were trained with cross-entropy loss, Adam optimizer [22] and learning rate of  $10^{-4}$  for 100 epochs.

### 5.1 CRF-simulator vs. real CRF-optimizer

We first evaluate the performance of our CRF Simulator. We report the accuracy with which CRF Simulator simulates the output of an actual CRF optimizer and analyze the energy of the labelings that CRF Simulator produces. We use the dataset described in Sec. 3.3.

#### 5.1.1 Accuracy

Our CRF Simulator CNN achieves 90.44% F-measure on the test data. Several examples obtained by CRF-simulator are shown in Fig. 5, along with the ground truth segmentations produced by the actual CRF optimizer. We selected examples for a small, medium, and large values of  $\lambda$ . The labelings produced by our simulator are not guaranteed to have the lowest energy, since energy is not a part

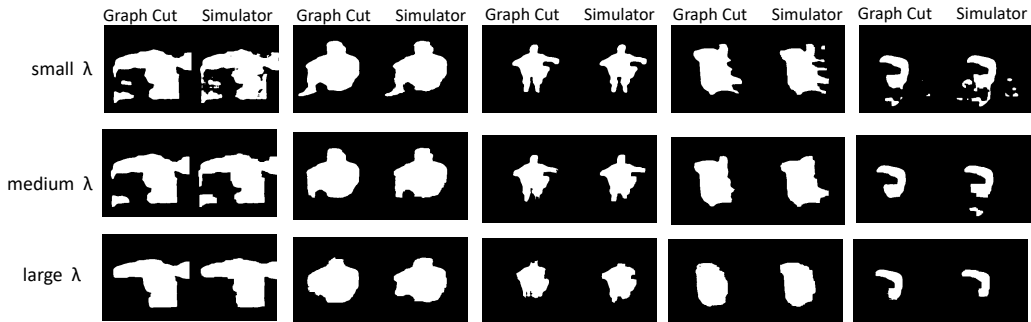


Figure 5: Illustrates some labellings learned by our CRF Simulator for small, medium, and large  $\lambda$  values. In each image, left part shows output of graph cut, and right part shows output of our simulator.

of training criteria. However, they capture the “spirit” of the regularization encoded into the energy in Eq. (1). For low  $\lambda$  values, the obtained labeling is noisy, as mostly unary terms are followed. For larger  $\lambda$ , noise and thin structures are smoothed out, holes are filled in, etc. One can argue that it is the spirit of the regularizer that one is after when performing energy optimization, and the actual energy value is of no interest by itself.

It is interesting to note that for  $\lambda = 0$ , our labelings do not follow the unary terms exactly, unlike the exact CRF optimizer. Our simulator still performs a small amount of regularization. This is, again, because our simulator learns to mimic the behavior of the actual optimizer instead of learning to produce the lowest energy labeling.

### 5.1.2 Energy

It is interesting to analyze the energy of the labelings produced by our CRF Simulator and compare to the energy of the optimal labelings produced by an actual CRF regularizer. Figure 6(left) shows scatter plots where each test image is a point, x-axis is the optimal energy obtained with graph-cut and y-axis is the energy computed for the labeling obtained with CRF-simulator. The plot in blue compares just the unary terms of the energy showing correlation coefficient of  $r = 0.98$ . The plot in green plots just the smoothness terms of the energy showing correlation coefficient of  $r = 0.61$ . Finally, the plot in red plots the total energy

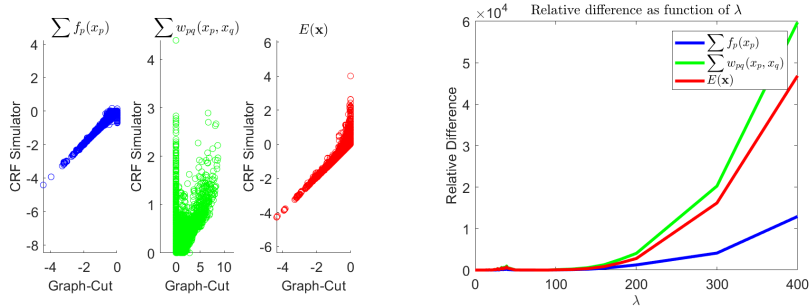


Figure 6: Left: Scatter plots illustrating correlation between the optimal energy and the energy obtained with CRF-simulator on the test images. Unary terms (with correlation coefficient  $r = 0.98$ ) are shown in blue, smoothness terms ( $r = 0.61$ ) in green and total energy ( $r = 0.93$ ) in red. Right: Average relative difference in energy as a function of regularization weight  $\lambda$ .

showing correlation coefficient of  $r = 0.93$ . Observe the region of the green scatter plot directly above graph-cut energy 0. This region dramatically reduces the correlation coefficient. It consists of images for which optimal solution is empty and therefore has zero smoothness term. This happens for high values of regularization weight  $\lambda$ . In such case, the learned solution is usually non-empty and has a non-zero discontinuity cost, reducing correlation. We further analyze the relative difference between the optimal and simulated energies as a function of regularization weight  $\lambda$ , see Fig. 6(right). Indeed, the relative difference grows as a function of  $\lambda$ . In practice however, we are interested in the lower range of values for the regularization weight  $\lambda$  where correlation of energies is high.

## 5.2 Complete System

In this section, we evaluate the performance of the complete end-to-end system that includes CRF-simulator component (Fig. 3). But first, for completeness, we report the performance of the Saliency-CNN alone (without post-processing) and with actual CRF optimizer postprocessing.

**Saliency CNN:** Our Saliency CNN achieves the F-measure of 88.21% on the task of saliency segmentation, when used on its own.

Saliency CNN	CRF optimizer	Complete TF	Complete TT	Complete FT	Complete FF	Comp
88.22	88.81	89.3	<b>89.40</b>	89.05	88.93	

Table 1:  $F$ -measure on the test data for the Saliency CNN, Saliency CNN with CRF Optimizer as post-processing, and our five Complete systems.

**Saliency CNN followed by CRF optimizer postprocessing:** Next we apply actual CRF optimizer as a postprocessing step. The results depend on the choice of  $\lambda$  in the energy function, which controls how much regularization is needed. In general, the the optimal value of  $\lambda$  varies between the images. However, when applying CRF Optimizer as post-processing, we must fix  $\lambda$  to a certain value. Choosing the best fixed value per dataset (using validation data),  $\lambda = 15$  gives the best performance, with the overall  $F$ -measure of 88.81%. A complete end-to-end trained system that uses our CRF Simulator (see Sec. 5.2) achieves a better  $F$ -measure of 89.40%

For CRF-optimizer, it is also interesting to measure what is the best  $F$ -measure that can be achieved if we choose the best  $\lambda$  for each image. While unrealistic in practice (best  $\lambda$  per image is not known), this gives an idea of how much improvement a regularizer can achieve if it was possible to learn best weights per each individual image. Going over all  $\lambda$ 's for each image, and choosing the one that gives the best  $F$ -measure for that image, gives the overall performance of 91.22%. Thus learning better weights would help the complete system performance.

**Complete System Variants:** We train our Complete System in five different regimes, depending on which CNN components have their weights fixed or allowed to be tuned during training. The parameters of our Weights CNN component are always trainable. The weights of Saliency CNN and CRF-Simulator CNN can either be fixed or trainable. This gives us four different combinations during training. The fifth regime is as follows. We allow all components to have trainable weights but initialize CRF Simulator weights to be random. This allows us to validate that the gains we have with CRF Simulator component are not just due to having a larger network.

Table 1 shows the  $F$ -measure on the test data for the Saliency CNN, Saliency CNN with CRF optimizer as post-processing, and our Complete System in five

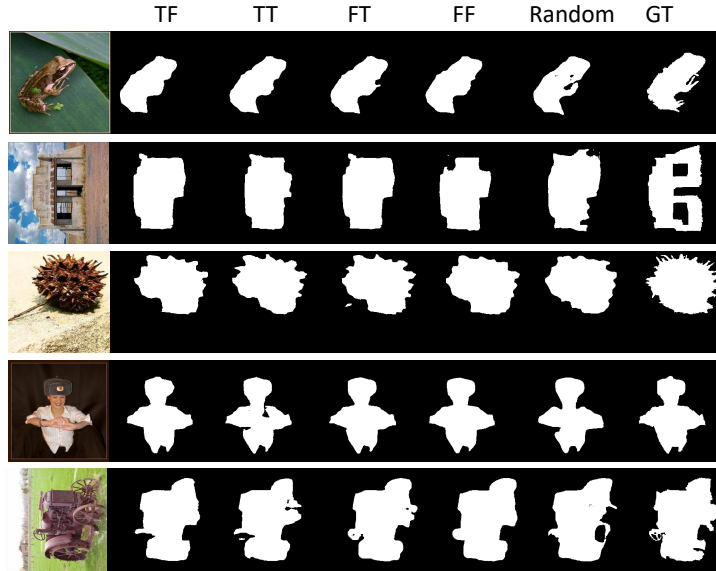


Figure 7: Some representative results of our Complete system.

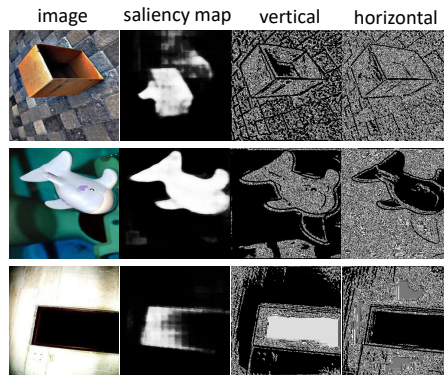


Figure 8: Edges learned by the complete system. From left to right: input image, saliency probabilities, vertical and horizontal  $w_{pq}$ .

different regimes. Two boolean flags after “Complete” specify which weights of the Complete system are fixed and which are allowed to be tuned. The first boolean flag corresponds to the Saliency CNN, and the second to the CRF Simulator. For example, “TF” means the Saliency CNN weights are tuned, while CRF Simulator weights are fixed. Finally, the last column shows the performance for our complete system when all the weights are tuned, but CRF Simulator weights are initialized to be random.

CRF Optimizer, used as post-processing, improves saliency results. The Complete system, initialized with random weights (last column in Table 1 ) is better than Saliency CNN alone, but actually worse than CRF Optimizer post-processing. This is not surprising since in this case, CRF Simulator module does not perform any regularization but only serves to enlarge a saliency network. All four variants of our Complete System with pre-trained CRF Simulator perform better than CRF Optimizer as post-processing. The best performance is in the “TT” case, since there are more tunable weights. The “TF” case is better than “FT” case. It is better to leave CRF Simulator weights unchanged but tune saliency weights as opposed to leaving Saliency weights fixed and tuning CRF Simulator weights. In the “TF” case, the complete system has a chance to fine-tune the Saliency module weights to suite better to the regularization transformations done by the CRF Simulator module.

Some labelings obtained by our Complete System are shown in Fig. 7. Observe that labelings produced by Complete System variants with fixed CRF Simulator (second and fifth column) capture the spirit of the CRF regularizer better. They even imitate the rectilinear nature of boundaries characteristics of four neighborhood CRF optimizer. Also observe that labelings in the “Random” column are the least regularized.

It is interesting to inspect weights  $w_{pq}$  learned by our Weight CNN module in Fig. 4. Consider some examples in Fig. 8. Here each row shows the input image, the saliency map, and the vertical and horizontal weights  $w_{pq}$  (brighter intensity means larger weight). For most training examples the learned horizontal and vertical weights  $w_{pq}$  resemble edges as shown in the top row of Fig. 8. For about a third of the data, the learned weights are similar to those shown in the second row of Fig. 8. Large portions of the background (for the vertical terms) and large portions inside the salient object (for horizontal terms) are of low cost with almost no edges detected. This might be because these images are particularly easy for saliency detection. It is possible that while Weights CNN module was designed to learn smoothness terms, it also learns about saliency to some degree. Therefore it does not have to detect edges in areas where it is easy to determine

whether the pixels belong to salient object or background. In a few very rare cases, the edges look like the bottom row in Fig. 8. This may be either failure to learn edges well. Or it may have something to do with the failure of the Saliency CNN (Fig. 2) to obtain a good saliency map. Notice in this case, the saliency map is missing a large portion of the object. The edge learning component may have imposed a large penalty on vertical weights to try to prevent the CRF Simulator cutting through the salient object.

## 6 Conclusions and Future Work

We presented a new approach for combining CNN and CRF in an end-to-end trainable system. The main idea is to simulate the regularization properties of an actual CRF optimizer by a special module. This module has a standard CNN architecture and is trained on examples produced by an actual CRF optimizer. The ground truth can be obtained in an unlimited quantity without user interaction, given an efficient CRF optimizer. The advantage of our approach over previous work is that we do not have to implement the complex mechanics of optimizing CRF as part of CNN.

In the future, we plan to investigate CRF-simulators for other energy/optimizer combinations. In particular, an interesting question is how well CRF-simulator performs for energies where the optimum solution cannot be computed exactly, and has to be approximated.

Another interesting direction is to design a better Weight CNN module for learning regularization weights. There is ample evidence that learning to adapt regularizer strength appropriately for each image can lead to significant performance gains.

## References

- [1] T. Ajanthan, A. Desmaison, R. Bunel, M. Salzmann, P. H. S. Torr, and M. P. Kumar. Efficient linear programming for dense crfs. In *CVPR*, pages 2934–2942. IEEE Computer Society, 2017.
- [2] A. Arnab, S. Jayasumana, S. Zheng, and P. H. S. Torr. Higher order potentials in end-to-end trainable conditional random fields. In *ECCV*, 2016.
- [3] A. Arnab, S. Zheng, S. Jayasumana, B. Romera-Paredes, M. Larsson, A. Kirillov, B. Savchynskyy, C. Rother, F. Kahl, and P. H. S. Torr. Conditional random fields



- meet deep neural networks for semantic segmentation: Combining probabilistic graphical models with deep learning for structured prediction. *IEEE Signal Process. Mag.*, 35(1):37–52, 2018.
- [4] Y. Boykov and G. Funka-Lea. Graph cuts and segmentation. *IJCV*, pages 109–131, 2006.
- [5] Y. Boykov and V. Kolmogorov. An experimental comparison of min-cut/max-flow algorithms for energy minimization in vision. In *EMMCVPR*, pages 359–374, 2001.
- [6] Y. Boykov, O. Veksler, and R. Zabih. Fast approximate energy minimization via graph cuts. *PAMI*, 23(11):1222–1239, November 2001.
- [7] S. Chandra and I. Kokkinos. Fast, exact and multi-scale inference for semantic image segmentation with deep gaussian crfs. In *European Conference on Computer Vision(ECCV)*, page 402418. Springer International Publishing, 2016.
- [8] S. Chandra, N. Usunier, and I. Kokkinos. Dense and low-rank gaussian crfs using deep embeddings. In *International Conference on Computer Vision (ICCV)*, volume 2, 2017.
- [9] L. Chen, G. Papandreou, I. Kokkinos, K. Murphy, and A. L. Yuille. Semantic image segmentation with deep convolutional nets and fully connected crfs. In *ICLR*, 2015.
- [10] L.-C. Chen, A. G. Schwing, A. L. Yuille, and R. Urtasun. Learning deep structured models. In *ICML*, 2015.
- [11] Z. Chen, X. Sun, L. Wang, Y. Yu, and C. Huang. A deep visual correspondence embedding model for stereo matching costs. In *2015 IEEE International Conference on Computer Vision (ICCV)*, volume 00, pages 972–980, Dec. 2015.
- [12] L. N. Clement Farabet, Camille Couprie and Y. LeCun. Learning hierarchical features for scene labeling. *IEEE Trans. on Pat. Anal. and Mach. Int.*, 2013. in press.
- [13] J. Deng, W. Dong, R. Socher, L.-J. Li, K. Li, and L. Fei-Fei. ImageNet: A Large-Scale Hierarchical Image Database. In *CVPR09*, 2009.
- [14] A. Desmaison, R. Bunel, P. Kohli, P. H. S. Torr, and M. P. Kumar. Efficient continuous relaxations for dense CRF. *CoRR*, abs/1608.06192, 2016.
- [15] J. Djolonga and A. Krause. Differentiable learning of submodular models. In I. Guyon, U. V. Luxburg, S. Bengio, H. Wallach, R. Fergus, S. Vishwanathan, and R. Garnett, editors, *Advances in Neural Information Processing Systems 30*, pages 1013–1023. 2017.
- [16] A. Dosovitskiy, P. Fischer, E. Ilg, P. Häusser, C. Hazirbas, V. Golkov, P. van der Smagt, D. Cremers, and T. Brox. FlowNet: Learning optical flow with convolutional networks. In *2015 IEEE International Conference on Computer Vision, ICCV 2015, Santiago, Chile, December 7-13, 2015*, pages 2758–2766, 2015.

- [17] M. Everingham, L. Van Gool, C. K. I. Williams, J. Winn, and A. Zisserman. The PASCAL Visual Object Classes Challenge 2012 (VOC2012) Results. <http://www.pascal-network.org/challenges/VOC/voc2012/workshop/index.html>.
- [18] K. Fukushima. Neocognitron: A self-organizing neural network model for a mechanism of pattern recognition unaffected by shift in position. *Biological Cybernetics*, 36(4):193–202, Apr 1980.
- [19] Q. Hou, M.-M. Cheng, X. Hu, A. Borji, Z. Tu, and P. Torr. Deeply supervised salient object detection with short connections. In *Conference on Computer Vision and Pattern Recognition (CVPR)*, pages 5300–5309. IEEE, 2017.
- [20] V. Jampani, M. Kiefel, and P. V. Gehler. Learning sparse high dimensional filters: Image filtering, dense crfs and bilateral neural networks. In *Conference on Computer Vision and Pattern Recognition*, pages 4452–4461, 2016.
- [21] J. H. Kappes, B. Andres, F. A. Hamprecht, C. Schnörr, S. Nowozin, D. Batra, S. Kim, B. X. Kausler, T. Kröger, J. Lellmann, N. Komodakis, B. Savchynskyy, and C. Rother. A comparative study of modern inference techniques for structured discrete energy minimization problems. *International Journal of Computer Vision*, pages 1–30, 2015.
- [22] D. P. Kingma and J. Ba. Adam: A method for stochastic optimization. *CoRR*, abs/1412.6980, 2014.
- [23] P. Knöbelreiter, C. Reinbacher, A. Shekhovtsov, and T. Pock. End-to-end training of hybrid CNN-CRF models for stereo. In *CVPR*, pages 1456–1465. IEEE Computer Society, 2017.
- [24] D. Koller and N. Friedman. *Probabilistic Graphical Models*. The MIT Press, 2009.
- [25] P. Krähenbühl and V. Koltun. Efficient inference in fully connected crfs with gaussian edge potentials. In *NIPS*, pages 109–117, 2011.
- [26] A. Krizhevsky, I. Sutskever, and G. E. Hinton. Imagenet classification with deep convolutional neural networks. In *NIPS*, 2012.
- [27] J. Lafferty, A. McCallum, and F. Pereira. Conditional random fields. In *ICML*, 2001.
- [28] Y. LeCun, B. Boser, J. S. Denker, D. Henderson, R. E. Howard, W. Hubbard, and L. D. Jackel. Backpropagation applied to handwritten zip code recognition. *Neural Comput.*, 1(4):541–551, December 1989.
- [29] Z. Li, Q. Chen, and V. Koltun. Interactive image segmentation with latent diversity. In *Proceedings of the IEEE Conference on Computer Vision and Pattern Recognition*, pages 577–585, 2018.
- [30] E. Shelhamer, J. Long, and T. Darrell. Fully convolutional networks for semantic segmentation. *IEEE Trans. Pattern Anal. Mach. Intell.*, 39(4):640–651, 2017.

- [31] K. Simonyan and A. Zisserman. Very deep convolutional networks for large-scale image recognition, 2014.
- [32] R. Szeliski, R. Zabih, D. Scharstein, O. Veksler, V. Kolmogorov, A. Agarwala, M. Tappen, and C. Rother. A comparative study of energy minimization methods for mrfs. *TPAMI*, 2008.
- [33] M. Tang, A. Djelouah, F. Perazzi, Y. Boykov, and C. Schroers. Normalized cut loss for weakly-supervised cnn segmentation. In *IEEE conference on Computer Vision and Pattern Recognition (CVPR), Salt Lake City*, 2018.
- [34] R. Vemulapalli, O. Tuzel, M. Liu, and R. Chellappa. Gaussian conditional random field network for semantic segmentation. In *Conference on Computer Vision and Pattern Recognition (CVPR)*, pages 3224–3233, June 2016.
- [35] J. Zbontar and Y. LeCun. Computing the stereo matching cost with a convolutional neural network. In *IEEE Conference on Computer Vision and Pattern Recognition, CVPR 2015, Boston, MA, USA, June 7-12, 2015*, pages 1592–1599, 2015.
- [36] N. Zheng, X. Tang, H. Shum, J. Wang, T. Liu, J. Sun, and Z. Yuan. Learning to detect a salient object. *IEEE Transactions on Pattern Analysis and Machine Intelligence*, 33:353–367, 2010.
- [37] S. Zheng, S. Jayasumana, B. Romera-Paredes, V. Vineet, Z. Su, D. Du, C. Huang, and P. Torr. Conditional random fields as recurrent neural networks. In *ICCV*, pages 1529–1537, 2015.